PAPER

Interplay of correlations and Majorana mode from local solution perspective

IOP Publishing Journal of Physics: Condensed Matter
J. Phys.: Condens. Matter **37** (2025) 055302 (12pp) https://doi.org/10.1088/1361-648X/ad8ea2

Interplay of correlations and Majorana mode from local solution perspective

Jan Barański[1,*], Magdalena Barańska[1], Tomasz Zienkiewicz[1] and Tadeusz Domański[2]

[1] Department of General Education, Polish Air Force University, ul. Dywizjonu 303 nr 35, 08521 Deblin, Poland
[2] Institute of Physics, M. Curie-Skłodowska University, 20-031 Lublin, Poland

E-mail: j.baranski@law.mil.pl, m.baranska@law.mil.pl, t.zienkiewicz@law.mil.pl and doman@kft.umcs.lublin.pl

Received 5 September 2024, revised 26 October 2024
Accepted for publication 4 November 2024
Published 18 November 2024

Abstract

We study the quasiparticle spectrum of a hybrid system, comprising a correlated (Anderson-type) quantum dot coupled to a topological superconducting nanowire hosting the Majorana boundary modes. From the exact solution of the low-energy effective Hamiltonian, we uncover a subtle interplay between Coulomb repulsion and the Majorana mode. Our analytical expressions show that the spectral weight of the leaking Majorana mode is sensitive to both the quantum dot energy level and the repulsive potential. We compare our results with estimations by Ricco *et al* (2019 *Phys. Rev.*B **99** 155159) obtained for the same hybrid structure using the Hubbard-type decoupling scheme, and analytically quantify the spectral weight of the zero-energy (topological) mode coexisting with the finite-energy (trivial) states of the quantum dot. We also show that empirical verification of these spectral weights could be feasible through spin-polarized Andreev spectroscopy.

Keywords: quantum dot, Majorana quasiparticle, SESAR

1. Introduction

Quantum dots side-attached to topological superconducting nanowires have been considered as a suitable platform for probing the Majorana boundary modes [1–7] which can demonstrate their non-local nature [8]. Hybridization between these constituents induces the intersite pairing, allowing for leakage of the Majorana mode onto the quantum dot region. Such a process has been initially predicted for the uncorrelated case [9] and later on also in the presence of Coulomb repulsion [10–17]. Distinguishing the Majorana zero modes (MZMs) from trivial states of the QD is, however, a challenging issue because various trivial states at zero energy could mimic the behavior of MZMs [8, 18].

Furthermore, in various hybrid structures the trivial states can coexist with topological ones [19, 20] and their signatures might potentially yield misleading conclusions. For example, Liu *et al* [21] demonstrated that coalescence of the Andreev states can enhance zero-bias conductance to $2e^2/h$, typical for the Majorana mode. Kondo resonance, appearing at zero energy in strongly correlated structures, could also be confused with the Majorana quasiparticle. Differences between these effects could be resolved by spin-polarized tunneling spectroscopy [10–14, 22–24], yet their unambiguous identification would be rather difficult.

Given these facts, there is an ultimate need to accurately describe the quasiparticle spectra in topological hybrid systems. To address this issue, we analyze here the minimal setup composed of the Anderson-type quantum impurity coupled to the Majorana mode (figure 1), which can be solved analytically. From the exact solution, we determine the eigenstates and analytically express the quasiparticle energies and their spectral weights, providing information about optimal conditions for leakage of the zero-energy Majorana mode onto the correlated quantum impurity with strong Coulomb

* Author to whom any correspondence should be addressed.

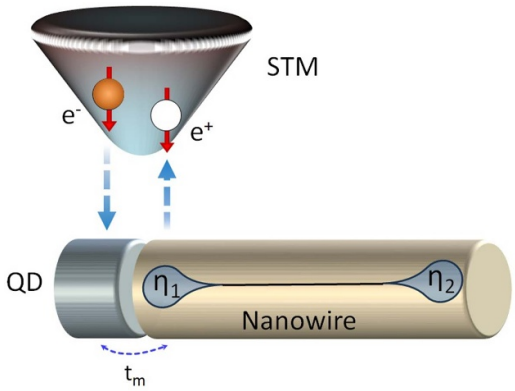

Figure 1. Schematics of the quantum dot (QD) attached to the topological nanowire, hosting the boundary Majorana modes η_i. Quasiparticles of the QD could be probed by spin-polarized scanning spectroscopy, measuring the conductance of the charge current contributed by electron-to-hole (Andreev) scattering of identical spins (marked by red arrows).

repulsion between opposite-spin electrons. Our study could be regarded as complementary to the previous investigations based either on the Hubbard-I decoupling scheme [7] or other purely numerical considerations [10–16]. Information derived from such analytical results could be useful for considerations of these quantum dot-topological superconductor hybrid structures under nonequilibrium conditions (for instance imposed by gate potentials or time-dependent driving) when precise knowledge of the eigenfunctions and quasiparticle energies is necessary to deduce the quantum evolution.

For experimental detection of the Majorana and the trivial bound states, we consider the Selective Equal-Spin Andreev Reflection (SESAR) spectroscopy. In contrast to ordinary Andreev reflection, its mechanism relies on polarized charge transfer by scattering an electron into a hole of the same spins. In quantum dot-Majorana hybrids, this process is feasible due to the intersite triplet pairing. Such a mechanism was proposed by He *et al* [25] for reliable identification of Majorana quasiparticles. Spin-polarized Andreev spectroscopy has also enabled the detection of topological zero-energy modes inside the vortex in a topological superconductor [26]. In subsequent studies, spin-dependent transport characteristics have been measured for magnetic atom chains, revealing inherent polarization of the Majorana quasiparticles at their edges [27]. SESAR has also been proposed for probing the spatial profile of Majorana quasiparticles in topological planar Josephson junctions [28].

Furthermore, the recent realization of the minimal Kitaev chain in double quantum dots interconnected through a conventional superconductor [29, 30] enabled the realization of triplet pairing, which has been resolved by spin-polarized crossed Andreev scattering [31]. Another platform for Majorana quasiparticles are topological nodal-point superconductors [32], where SESAR spectroscopy has been used as well. Motivated by the popular use of spin-resolved Andreev spectroscopy, we inspect its mechanism here in the minimal QD-MBS setup, providing the exact Green's functions, which encode information on the SESAR processes.

It has been established [33] that charge tunneling could probe the lifetime of the Majorana states in heterostructures consisting of a metal-quantum dot-topological superconductor. Charge transfer varies the electron number on the quantum dot by ± 1, thus connecting the even and odd parity sections. In what follows, we determine the probability of such parity changes in the strongly correlated quantum dot. This brings information concerning optimal conditions for the leakage of the Majorana modes.

The paper is organized as follows. In section 2 we introduce the model and present the general forms of its eigenstates and eigenenergies for arbitrary overlap between the Majorana boundary modes. Next, in section 3, we analyze the spin-resolved quasiparticle spectra of the correlated QD coupled only to one Majorana mode. The next section 4 generalizes our treatment to the case with nonzero overlap between the Majorana modes. Finally, we summarize the obtained results. The appendix provides brief information concerning the role of the magnetic field.

2. Eigenstates and eigenenergies

The low-energy physics of the hybrid structure shown in figure 1 can be described by the following Hamiltonian:

$$\hat{H} = \hat{H}_{\mathrm{QD}} + \lambda\left(\hat{d}_{\downarrow}^{\dagger}\hat{\eta}_1 + \hat{\eta}_1\hat{d}_{\downarrow}\right) + i\epsilon_m\hat{\eta}_1\hat{\eta}_2, \tag{1}$$

where

$$\hat{H}_{\mathrm{QD}} = \sum_{\sigma}\varepsilon_d\hat{d}_{\sigma}^{\dagger}\hat{d}_{\sigma} + U_d\hat{n}_{\uparrow}\hat{n}_{\downarrow} \tag{2}$$

refers to the correlated quantum dot (QD) with the energy level ε_d and the Coulomb potential U_d. The second term on the r.h.s. of equation (1) describes the coupling of the QD to one of the boundary states, $\hat{\eta}_1$, of the topological nanowire. In the analyzed model, we assume that the tunneling between the dot and the MZM is spin-polarized. This is because Majorana modes in topological superconductors are typically associated with a specific spin polarization, depending on the direction of the magnetic field and the spin-orbit interaction. The boundary modes are described by self-hermitian operators $\hat{\eta}_i^{\dagger} = \hat{\eta}_i$. The last term stands for an overlap between the Majorana modes $(\hat{\eta}_1, \hat{\eta}_2)$ and it is relevant to short topological nanowires.

It is convenient to express the Majorana operators in terms of the conventional fermion operators $\hat{f}, \hat{f}^{\dagger}$ defined through $\hat{\eta}_1 = \frac{1}{\sqrt{2}}(\hat{f}^{\dagger} + \hat{f})$ and $\hat{\eta}_2 = \frac{i}{\sqrt{2}}(\hat{f}^{\dagger} - \hat{f})$. Hamiltonian (1) then acquires the following structure:

$$\begin{aligned}\hat{H} = \hat{H}_{QD} &+ t_m\left(\hat{d}_{\downarrow}^{\dagger}\hat{f} + \hat{f}^{\dagger}\hat{d}_{\downarrow}\right) \\ &+ t_m\left(\hat{d}_{\downarrow}^{\dagger}\hat{f}^{\dagger} + \hat{f}\hat{d}_{\downarrow}\right) + \epsilon_m\left(\hat{f}^{\dagger}\hat{f} - \frac{1}{2}\right),\end{aligned} \tag{3}$$

where $t_m = \lambda/\sqrt{2}$. We note that the second part of this Hamiltonian (3) represents the usual tunneling of a spin-↓

electron between the QD and the topological nanowire, while the third part represents the intersite pairing potential, where triplet pairs are formed or annihilated.

The Hilbert space of the model Hamiltonian (3) is spanned by eight states $|n_{d\sigma}, n_f\rangle$. Its eigenstates can be determined analytically and are represented by the following superpositions:

$$|\Psi_1^{\pm}\rangle = u_1^{\pm}|0,0\rangle + v_1^{\pm}|\downarrow,1\rangle, \tag{4}$$
$$|\Psi_2^{\pm}\rangle = u_2^{\pm}|\downarrow,0\rangle + v_2^{\pm}|0,1\rangle, \tag{5}$$
$$|\Psi_3^{\pm}\rangle = u_3^{\pm}|\uparrow\downarrow,0\rangle + v_3^{\pm}|\uparrow,1\rangle, \tag{6}$$
$$|\Psi_4^{\pm}\rangle = u_4^{\pm}|\uparrow,0\rangle + v_4^{\pm}|\uparrow\downarrow,1\rangle. \tag{7}$$

Let us remark that the correlated quantum dot coupled to a conventional superconductor would be characterized by a different set of eigenvectors, represented either by the singly occupied configurations $|\uparrow\rangle$ and $|\downarrow\rangle$ or the BCS-type coherent superpositions $u^{\pm}|0\rangle + v^{\pm}|\uparrow\downarrow\rangle$ [34, 35]. Here, in contrast, we obtain eigenstates that are superpositions of either the empty and singly occupied dot, $|\Psi_{1,2}\rangle$, or the doubly and singly occupied dot, $|\Psi_{3,4}\rangle$, combined with the edge mode. Unlike the mentioned BCS-type superpositions, the eigenstates of the considered system are superpositions of states with different dot electron parity. One can also note that the states $|\Psi_{1,2}\rangle$ are characterized by opposite dot magnetization compared to states $|\Psi_{3,4}\rangle$. Consequently, a ground state transition from $|\Psi_{1,2}\rangle$ to $|\Psi_{3,4}\rangle$ (or vice versa) is accompanied by a conversion of the dot's magnetic properties (c.f. figure 2). Such a set of eigenfunctions originates from the intersite pairing. For each of these configurations, we obtained two possible solutions, $\hat{H}|\Psi_i^{\pm}\rangle = E_i^{\pm}|\Psi_i^{\pm}\rangle$, with eigenvalues

$$E_1^{\pm} = \frac{1}{2}\left[\epsilon_d \pm \sqrt{(\epsilon_d+\epsilon_m)^2 + 4t_m^2}\right], \tag{8}$$
$$E_2^{\pm} = \frac{1}{2}\left[\epsilon_d \pm \sqrt{(\epsilon_d-\epsilon_m)^2 + 4t_m^2}\right], \tag{9}$$
$$E_3^{\pm} = \frac{1}{2}\left[3\epsilon_d + U_d \pm \sqrt{(\epsilon_d-\epsilon_m+U_d)^2 + 4t_m^2}\right], \tag{10}$$
$$E_4^{\pm} = \frac{1}{2}\left[3\epsilon_d + U_d \pm \sqrt{(\epsilon_d+\epsilon_m+U_d)^2 + 4t_m^2}\right]. \tag{11}$$

As the values of the square roots are positive, therefore candidates for the ground state are only those eigenenergies (8)–(11) with a minus-sign in front of the square root.

Figure 2 illustrates these eigenenergies, indicating the ground state energy (solid line) obtained for large overlap between the QD and the Majorana modes, $\epsilon_m = 0.5U_d$. The dashed faded lines mark the eigenvalues of the excited states. The eigenenergies are plotted with respect to the parameter $\xi_d = \epsilon_d + \frac{U_d}{2}$, which represents the departure from the half-filled QD. In figure 2 we used the on-site Coulomb repulsion as the energy unit in order to highlight the critical points at which the ground state is represented by different types of states. Note that configurations $|\Psi_3\rangle$ and $|\Psi_4\rangle$ have a component related to the double QD occupancy, while for the states $|\Psi_1\rangle$ and $|\Psi_2\rangle$ a maximum number of electrons on the QD

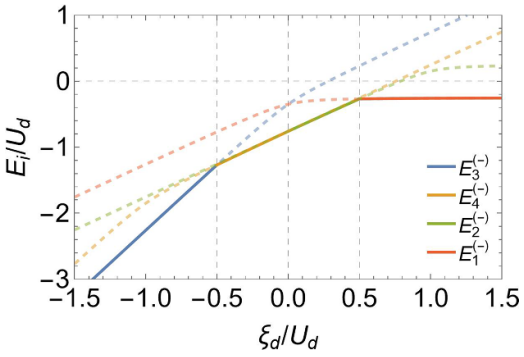

Figure 2. Dependence of the eigenenergies E_i^- on the energy level ε_d of the QD. Solid lines refer to the ground-state energy. Results are obtained for $t_m = 0.1U_d$ and $\epsilon_m = 0.5U_d$. Dashed faded lines represent excited states.

is one. Therefore, below QD half-filling ($\xi_d < 0$) the ground state is represented either by $|\Psi_3\rangle$ or $|\Psi_4\rangle$. In the opposite case, the Coulomb potential imposes the ground state $|\Psi_1\rangle$ or $|\Psi_2\rangle$.

In what follows, we shall inspect the quasiparticle excitation spectrum that could be probed by tunneling experiments when our hybrid structure is contacted with a conducting tip. The main purpose of this study is to evaluate the spectral weights shared between the topological and trivial branches, upon varying the energy level of the correlated QD.

3. Results for $\epsilon_m = 0$

Let us start with the situation corresponding to a sufficiently long topological nanowire where the overlap between the Majorana modes is negligible, $\epsilon_m \to 0$. Under such circumstances, $E_1^{\pm} = E_2^{\pm}$ and $E_3^{\pm} = E_4^{\pm}$ (nonvanishing overlap ϵ_m lifts this degeneracy). For a positive value $\epsilon_m > 0$, the ground state energy depends on the QD level ε_d and the Coulomb potential U_d.

$$\min E_i^- = \begin{cases} E_3^- & \text{for} \quad \xi_d \leqslant -U_d/2, \\ E_4^- & \text{for} \quad -U_d/2 < \xi_d \leqslant 0, \\ E_2^- & \text{for} \quad 0 < \xi_d \leqslant U_d/2, \\ E_1^- & \text{for} \quad U_d/2 < \xi_d. \end{cases} \tag{12}$$

To characterize the excitation spectrum of our hybrid system, it is convenient to introduce the abbreviations.

$$E_p = \sqrt{(\xi_d - U_d/2)^2 + 4t_m^2} \tag{13}$$
$$E_q = \sqrt{(\xi_d + U_d/2)^2 + 4t_m^2} \tag{14}$$

and define the coefficients

$$u_p^2 = \frac{1}{2}\left[1 + \frac{\xi_d - U_d/2}{E_p}\right] = 1 - v_p^2, \tag{15}$$
$$u_q^2 = \frac{1}{2}\left[1 + \frac{\xi_d + U_d/2}{E_p}\right] = 1 - v_q^2. \tag{16}$$

For $\epsilon_m = 0$ the eigenvectors (4)–(7) simplify to

$$|\Psi_1^-\rangle = u_p|0,0\rangle + v_p|\downarrow,1\rangle, \tag{17}$$
$$|\Psi_1^+\rangle = v_p|0,0\rangle - u_p|\downarrow,1\rangle, \tag{18}$$
$$|\Psi_2^-\rangle = v_p|\downarrow,0\rangle + u_p|0,1\rangle, \tag{19}$$
$$|\Psi_2^+\rangle = u_p|\downarrow,0\rangle - v_p|0,1\rangle, \tag{20}$$
$$|\Psi_3^-\rangle = v_q|\uparrow\downarrow,0\rangle + u_q|\uparrow,1\rangle, \tag{21}$$
$$|\Psi_3^+\rangle = u_q|\uparrow\downarrow,0\rangle - v_q|\uparrow,1\rangle, \tag{22}$$
$$|\Psi_4^-\rangle = u_q|\uparrow,0\rangle + v_q|\uparrow\downarrow,1\rangle, \tag{23}$$
$$|\Psi_4^+\rangle = v_q|\uparrow,0\rangle - u_q|\uparrow\downarrow,1\rangle. \tag{24}$$

Explicit expressions for $\epsilon_m \neq 0$ are discussed in section 4.

From the set of eigenvectors (17)–(24) and eigenenergies (8)–(11), we can construct arbitrary Green's functions, using the spectral Lehmann representation. We assume our setup to be in thermal equilibrium with an external bath, for instance, the substrate on which the topological nanowire is deposited and/or the conducting STM tip.

3.1. Spectrum of spin-↓ electrons

The Fourier transform of the single-particle propagator of spin-↓ electrons is given by

$$\langle\langle \hat{d}_\downarrow; \hat{d}_\downarrow^\dagger \rangle\rangle_\omega = \frac{1}{Z}\sum_{m,n,s,\bar{s}} |\langle \Psi_m^{\bar{s}}|\hat{d}_\downarrow|\Psi_n^s\rangle|^2 \frac{e^{-\beta E_n^s} + e^{-\beta E_m^{\bar{s}}}}{\omega + E_n^s - E_m^{\bar{s}}}, \tag{25}$$

where $Z = \sum_{n,s}\exp(-\beta E_n^s)$ denotes the partition function and $\beta = (k_B T)^{-1}$ is the inverse temperature. Indices $m,n = 1,2,3,4$ and s, $\bar{s} = \pm$ denote particular states introduced in equations (17)–(24) as well as their corresponding energies $E_{m/n}^{s/\bar{s}}$ given by equations (8)–(11). Transitions $\langle\Psi_m^{\bar{s}}|\hat{d}_\downarrow|\Psi_n^s\rangle$ are allowed only between the different parity states $\Psi_1^s \leftrightarrow \Psi_2^{\bar{s}}$ and $\Psi_3^s \leftrightarrow \Psi_4^{\bar{s}}$. Contribution to the zero-energy mode is given by transitions between degenerate states. Such degeneration occurs between particular states with the same indices ($s = \bar{s}$) as $E_1^\pm = E_2^\pm$ and $E_3^\pm = E_4^\pm$. Matrix elements of such transitions are given by $|\langle\Psi_1^+|\hat{d}_\downarrow|\Psi_2^+\rangle|^2 = |\langle\Psi_1^-|d_\downarrow|\Psi_2^-\rangle|^2 = u_p^2 v_p^2$ and $|\langle\Psi_3^-|d_\downarrow|\Psi_4^+\rangle|^2 = |\langle\Psi_3^+|\hat{d}_\downarrow|\Psi_4^-\rangle|^2 = u_q^2 v_q^2$. Therefore, the zero-energy pole contribution to the Green's function can be written as

$$\frac{1}{Z}\sum_{m,n}\sum_{s} |\langle\Psi_n^s|\hat{d}_\downarrow|\Psi_m^s\rangle|^2 \frac{e^{-\beta E_n^s} + e^{-\beta E_m^s}}{\omega + E_n^s - E_m^s} = \frac{A_1}{\omega + i0^+} \tag{26}$$

with the spectral weight

$$A_1 = \frac{4}{Z}\sum_{s=\pm}\left[u_p^2 v_p^2\left(e^{-\beta E_1^s}\right) + u_q^2 v_q^2\left(e^{-\beta E_3^s}\right)\right]. \tag{27}$$

On the other hand, transitions between the states $\Psi_1^s \leftrightarrow \Psi_2^{\bar{s}}$ and $\Psi_3^s \leftrightarrow \Psi_4^{\bar{s}}$ with different sign index $s \neq \bar{s}$ contribute to the finite-energy poles at $\pm E_p$ and $\pm E_q$, respectively. For $\Psi_1^s \leftrightarrow \Psi_2^{\bar{s}}$ matrix elements are given by $|\langle\Psi_1^+|d_\downarrow|\Psi_2^-\rangle|^2 = |\langle\Psi_2^+|d_\downarrow|\Psi_1^-\rangle|^2 = v_p^4$ and $|\langle\Psi_1^-|d_\downarrow|\Psi_2^+\rangle|^2 = |\langle\Psi_2^-|d_\downarrow|\Psi_1^+\rangle|^2 = u_p^4$. The contribution to the Green's function from the first two transitions takes the form:

$$\frac{1}{Z}\sum_{n,m=1,2} |\langle\Psi_n^+|\hat{d}_\downarrow|\Psi_m^-\rangle|^2 \frac{e^{-\beta E_n^+} + e^{-\beta E_m^-}}{\omega + E_n^+ - E_m^-} = 2\frac{v_p^4}{Z}\frac{e^{-\beta E_1^+} + e^{-\beta E_1^-}}{\omega + E_p} = \frac{2}{Z}\sum_{s=\pm} v_p^4 \frac{e^{-\beta E_1^s}}{\omega + E_p}. \tag{28}$$

Similarly, for the latter two we have

$$\frac{1}{Z}\sum_{n,m=1,2} |\langle\Psi_n^-|\hat{d}_\downarrow|\Psi_m^+\rangle|^2 \frac{e^{-\beta E_n^-} + e^{-\beta E_m^+}}{\omega + E_n^+ - E_m^-} = \frac{2}{Z}\sum_{s=\pm} u_p^4 \frac{e^{-\beta E_1^s}}{\omega - E_p}. \tag{29}$$

The total contribution to the trivial states from all transitions between $\Psi_1^s \leftrightarrow \Psi_2^{\bar{s}}$ can thus be written as

$$\frac{1}{Z}\sum_{m,n}^{1,2}\sum_{s=\pm} |\langle\Psi_n^s|\hat{d}_\downarrow|\Psi_m^{-s}\rangle|^2 \frac{e^{-\beta E_n} + e^{-\beta E_m}}{\omega + E_n - E_m} = \frac{A_2}{\omega + E_p + i0^+} + \frac{A_3}{\omega - E_p + i0^+}, \tag{30}$$

with amplitudes

$$A_2 = \frac{2}{Z}\sum_{s=\pm} u_p^4 e^{-\beta E_1^s} \tag{31}$$

$$A_3 = \frac{2}{Z}\sum_{s=\pm} v_p^4 e^{-\beta E_1^s}. \tag{32}$$

Analogous calculations for m and $n = 3,4$ give

$$\sum_{m,n}^{3,4}\sum_{s=\pm} |\langle\Psi_n^s|\hat{d}_\downarrow|\Psi_m^{-s}\rangle|^2 \frac{e^{-\beta E_n} + e^{-\beta E_m}}{\omega + E_n - E_m} = \frac{A_4}{\omega + E_q + i0^+} + \frac{A_5}{\omega - E_q + i0^+} \tag{33}$$

with amplitudes

$$A_4 = \frac{2}{Z}\sum_{s=\pm} u_q^4 e^{-\beta E_3^s}, \tag{34}$$

$$A_5 = \frac{2}{Z}\sum_{s=\pm} v_q^4 e^{-\beta E_3^s}. \tag{35}$$

The density of states $\rho_\downarrow(\omega) = -\frac{1}{\pi}\mathrm{Im}\langle\langle \hat{d}_\downarrow; \hat{d}_\downarrow^\dagger\rangle\rangle_{\omega+i0^+}$ of spin-↓ electrons consists of five branches

$$\rho_\downarrow(\omega) = A_1\delta(\omega) + A_2\delta(\omega - E_p) + A_3\delta(\omega + E_p) + A_4\delta(\omega - E_q) + A_5\delta(\omega + E_q), \tag{36}$$

where A_1 represents the spectral weight of the Majorana mode transmitted onto the correlated quantum dot, and the amplitudes A_{2-5} refer to the trivial (finite-energy) quasiparticles. The coefficients A_i represent the spectral weights of the given

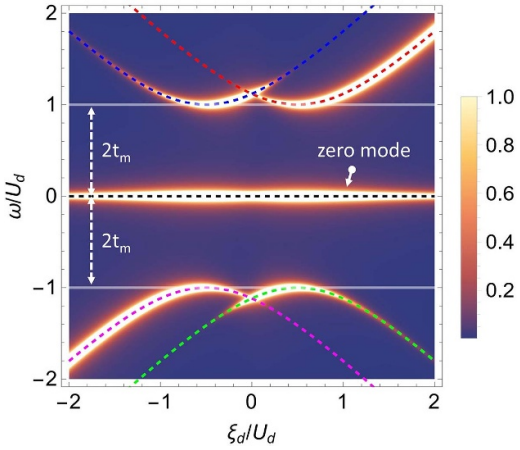

Figure 3. Five quasiparticle branches of the spin-resolved spectrum $\rho_{d\downarrow}(\omega)$ vary with respect to $\xi_d = \varepsilon_d + U_d/2$. Dashed lines show the quasiparticle energies, and their spectral weights, A_i, are displayed according to the r.h.s. bar scale. White faded lines indicate the topological gap separating ordinary states from the induced zero mode.

quasiparticles. In other words, these dimensionless numbers (A_i) can be regarded as probabilities for the existence of the quasiparticles at the energies ω_i. The total spectral weight satisfies the sum rule $\sum_{i=1}^{5} A_i = 1$.

Figure 3 shows the typical spectrum of $\downarrow$-spin electrons. The black dashed line indicates the zero-energy quasiparticle, originating from the Majorana mode leakage. Red/green dashed lines correspond to the quasiparticle energies $\pm E_p$ and blue/magenta indicate the quasiparticle energies $\pm E_q$, respectively. To understand their physical meaning, let us recall that an isolated QD ($t_m = 0$) has two quasiparticle energies: at $\omega = \varepsilon_d$ (i.e. $\xi_d = -\frac{U_d}{2}$) with spectral weight $1 - n_{d\sigma}$ and another Coulomb satellite at $\omega = \varepsilon_d + U_d$ (i.e. $\xi_d = \frac{U_d}{2}$) with spectral weight $n_{d\sigma}$. For $t_m \neq 0$, these quasiparticle branches evolve into the trivial modes $\pm E_p$ and $\pm E_q$ of our setup, which are gapped due to the intersite pairing (for details see section 3.4). In figure 3, we clearly notice *avoided-crossing* behavior of the trivial (finite-energy) quasiparticle branches, repelled at some distance from the topological (zero-energy) mode, which is due to the protection of the Majorana state. At the critical points, $\xi_d = \pm\frac{U_d}{2}$, the trivial states are separated from the zero-energy mode by a gap of $2t_m$. Furthermore, the spectral weight A_1 of the zero-energy mode, $\omega = 0$, is enhanced around $\omega = \xi_d - \frac{U_d}{2}$ and $\omega = \xi_d + \frac{U_d}{2}$.

To specify the optimal spectral weight of the Majorana mode, we present in figures 4 and 5 the variation of all amplitudes A_i against ξ_d. These plots demonstrate that, for the weak coupling t_m, practically only two trivial quasiparticles coexist with the zero-energy mode. In other words, the spectrum of $\downarrow$-spin electrons exhibits three dominant (out of five) quasiparticle branches. As regards the zero-energy mode, its optimal spectral weight coincides with $\xi_d = -\frac{U_d}{2}$ and $\xi_d = \frac{U_d}{2}$.

Figure 4 shows the influence of the coupling t_m on the energy region in which the Majorana spectral weight is noticeable. For infinitesimal coupling t_m, the Majorana mode exists only very close to the quasiparticle energies $\xi_d \pm \frac{U_d}{2}$. Upon

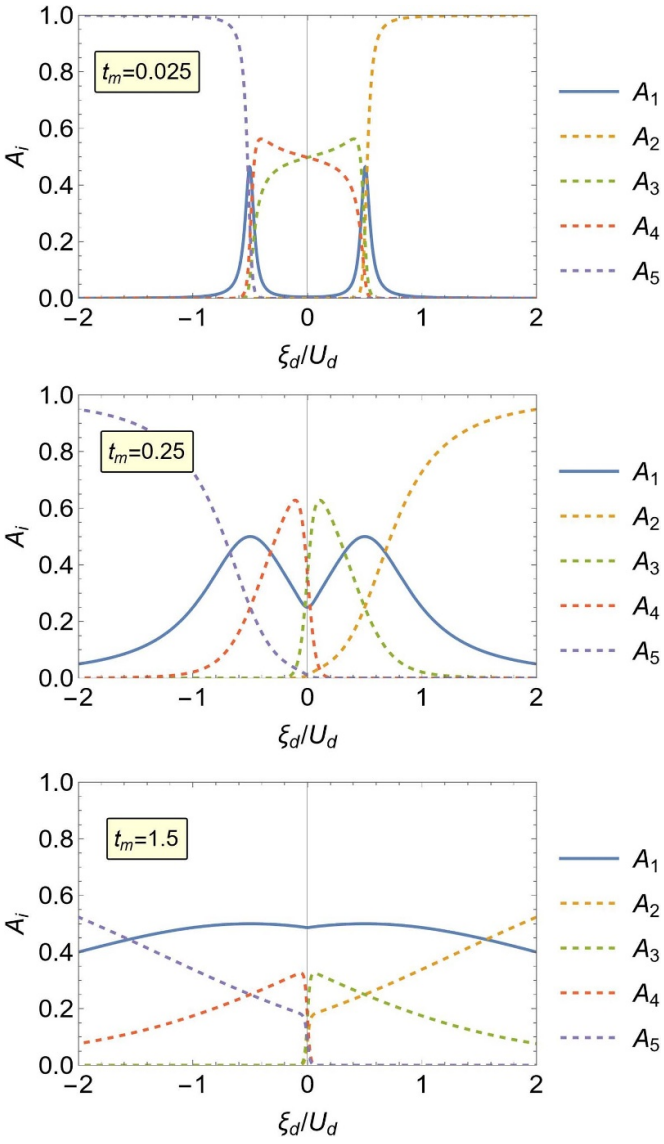

Figure 4. Variation of the spectral weights A_{1-5} against the QD energy level obtained for the weak coupling $t_m/U_d = 0.025$ (top panel), intermediate hybridization $t_m/U_d = 0.25$ (middle panel), and in the strong coupling limit $t_m/U_d = 1.5$ (bottom panel).

increasing t_m, the Majorana mode extends onto a much broader region around those energies. In the case of very strong dot-Majorana coupling ($t_m > U_d$), the quantum dot can be considered as an additional atom embedded in the topological chain. For such a "molecular" case, leakage of MZM is efficient over a wide range of ξ_d (c.f. bottom panel of figure 4). Let us remark that the optimal value, $\max\{A_1\} = 0.5$, coincides with the minima of $|E_{q,p}|$.

Similar behavior is observed when inspecting the influence of the Coulomb potential U_d, figure 5. In particular, at half-filling ($\xi_d = 0$), the spectral weight of the Majorana mode approaches its optimal value only for vanishing Coulomb repulsion $U_d \to 0$. For stronger Coulomb potential, the optimal spectral weight of the Majorana mode shifts from half-filling (as can be observed in the density of states, figure 3). We have checked that for $U_d = 4t_m$, the quasiparticle

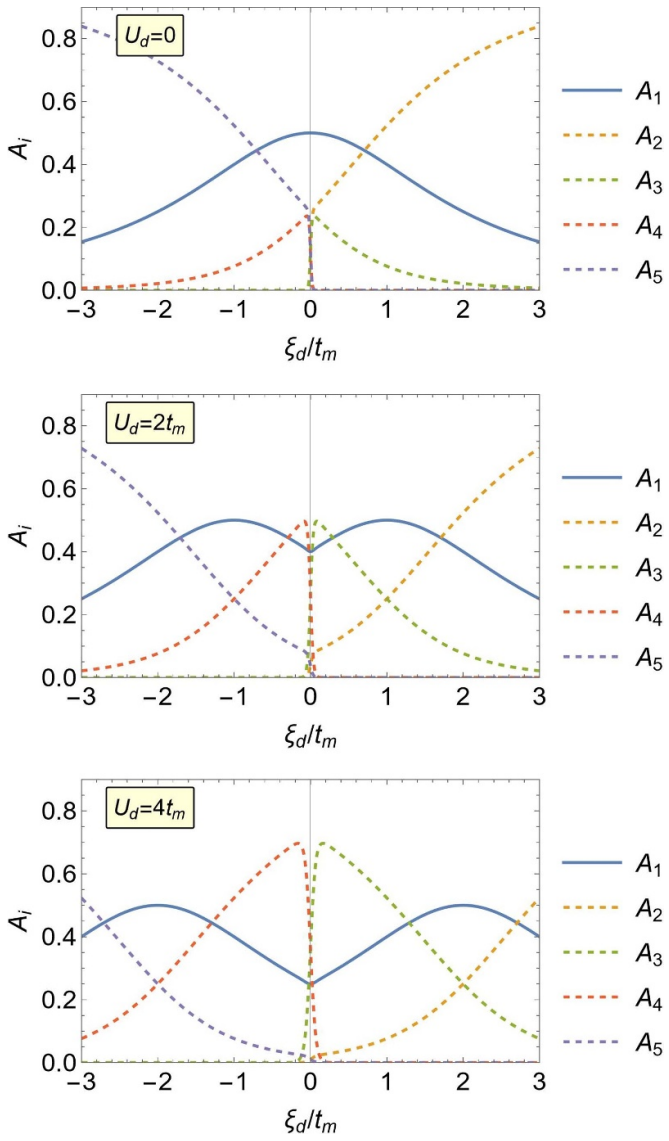

Figure 5. Variation of the spectral weights A_i with respect to the quantum dot energy level $\xi_d = \varepsilon_d + U_d/2$ obtained for several values of the Coulomb potential U_d, as indicated.

spectral weights at half-filling acquire the following values: $A_1 = 0.25, A_2 = A_5 \simeq 0.01, A_3 = A_4 \simeq 0.0365$. At half-filling, the effectiveness of MZM leakage diminishes with increasing correlation strength U_d. The maximal value of the spectral weight of A_1 (reaching 0.5) is preserved upon strong correlations when $\xi_d = \pm\frac{U_d}{2}$.

3.2. Spectrum of spin−↑ electrons

The excitation spectrum of ↑−electrons reveals qualitatively different behavior, even though the interaction term, $U_d\hat{n}_\uparrow\hat{n}_\downarrow$, mixes both spin sectors. The single-particle Green's function $\langle\langle\hat{d}_\uparrow;\hat{d}^\dagger_\uparrow\rangle\rangle_\omega$ can be expressed in a form analogous to equation (25). The only nonvanishing matrix elements are contributed by $\langle\Psi^s_2|\hat{d}_\uparrow|\Psi^{s'}_3\rangle$ and $\langle\Psi^s_1|\hat{d}_\uparrow|\Psi^{s'}_4\rangle$. We note that for $\epsilon_m = 0$ the pairs of quasiparticles appearing in these elements are not degenerate. For this reason, we observe four branches of the trivial quasiparticles (instead of two typical for the isolated QD). The spectrum of ↑ electrons does not show the presence of the Majorana mode, which should be pinned to zero energy. Degenerate pairs of the eigenstates $\Psi^\pm_1$, $\Psi^\pm_2$, and $\Psi^\pm_3$, $\Psi^\pm_4$ (in the case $\epsilon_m = 0$) imply that components of the Green function obtained from the matrix elements $\langle\Psi^s_2|\hat{d}_\uparrow|\Psi^{s'}_3\rangle$ are identical to those originating from $\langle\Psi^s_1|\hat{d}_\uparrow|\Psi^{s'}_4\rangle$. Accordingly, we obtain the following four-pole structure of the Green's function:

$$\begin{aligned}\langle\langle\hat{d}_\uparrow;\hat{d}^\dagger_\uparrow\rangle\rangle_\omega = &\frac{B_1}{\omega-\xi_d+\frac{1}{2}(E_p+E_q)}\\ &+\frac{B_2}{\omega-\xi_d-\frac{1}{2}(E_p+E_q)}\\ &+\frac{B_3}{\omega-\xi_d+\frac{1}{2}(E_p-E_q)}\\ &+\frac{B_4}{\omega-\xi_d-\frac{1}{2}(E_p-E_q)},\end{aligned} \tag{37}$$

with the amplitudes

$$B_1 = \frac{2}{Z}(v_pu_q - u_pv_q)^2\left(e^{-\beta E^+_1}+e^{-\beta E^-_3}\right), \tag{38}$$

$$B_2 = \frac{2}{Z}(u_pv_q - v_pu_q)^2\left(e^{-\beta E^-_1}+e^{-\beta E^+_3}\right), \tag{39}$$

$$B_3 = \frac{2}{Z}(u_pu_q + v_pv_q)^2\left(e^{-\beta E^+_1}+e^{-\beta E^+_3}\right), \tag{40}$$

$$B_4 = \frac{2}{Z}(u_pu_q + v_pv_q)^2\left(e^{-\beta E^-_1}+e^{-\beta E^-_3}\right). \tag{41}$$

In the energy region $\varepsilon_d \in (-U_d, 0)$, two amplitudes B_3 and B_4 are negligibly small, so the dominant contribution comes from B_1 and B_2. Outside of this regime, the prevailing contributions are from B_3 and B_4.

Figure 6 displays the spectrum of ↑−spin electrons obtained for the same set of parameters as in figure 3. We clearly notice the absence of the Majorana mode. Although ↑ electrons are not directly coupled to the MZM in the considered model, MZM leakage to ↓ electrons affects the opposite spin spectrum through electron correlations (U_d). Comparing the obtained results to the case where the MZM is completely absent $(t_m = 0)$, we observe that instead of two ordinary states located at $\omega = \xi_d \pm \frac{U_d}{2}$, we obtain four branches. The most pronounced branch, represented by the blue dashed line in figure 6 (corresponding to transitions between the states $\Psi^-_1 \leftrightarrow \Psi^-_3$ and $\Psi^-_2 \leftrightarrow \Psi^-_4$), reproduces the state located at $\omega = \xi_d - \frac{U_d}{2}$ for fillings way above 0.5 (i.e. $\xi_d \ll 0$) and the state at $\omega = \xi_d + \frac{U_d}{2}$ in the opposite case. Near half-filling, this state crosses the zero-energy level. The branch represented by the orange line behaves in the opposite manner, crossing zero energy under the same conditions, but with an inverse dependence on the filling. Two quasiparticle branches crossing at zero energy for half-filling, $\xi_d = 0$, have nothing to do with the topological mode. The influence of the topological superconductor is merely responsible for doubling the

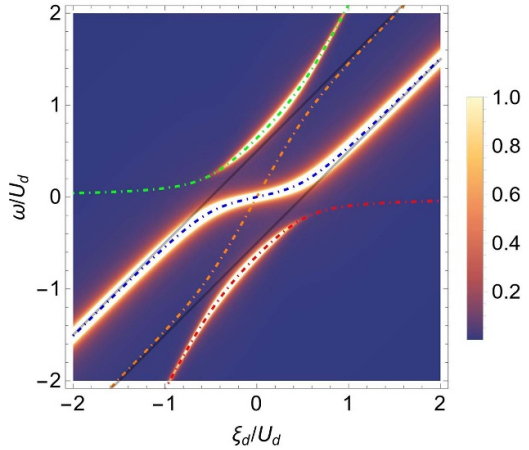

Figure 6. Variation of the quasiparticle spectrum $\rho_{d\uparrow}(\omega)$ with respect to $\xi_d = \varepsilon_d + U_d/2$ obtained for $t_m = 0.2U_d$. The dashed lines mark the positions of four poles, and their spectral weights are displayed by color-width, whose scale is indicated by the r.h.s. bar. Black faded lines mark the position of two poles $\omega = \xi_d \pm \frac{U_d}{2}$, which remain in the case $t_m = 0$.

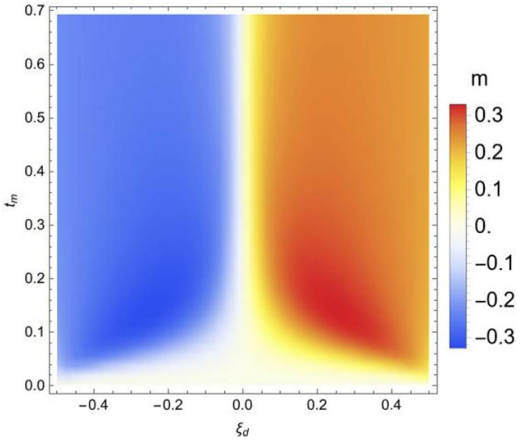

Figure 7. Magnetization of QD as function of $\xi_d = \varepsilon_d + \frac{U_d}{2}$ and the hybridization stregth t_m.

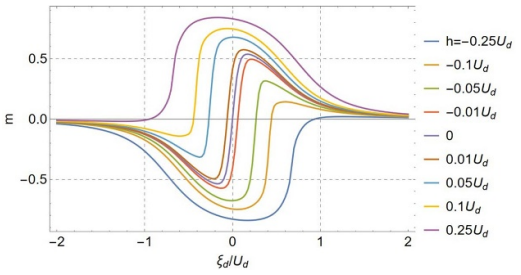

Figure 8. Magnetization of QD as function of $\xi_d = \varepsilon_d + \frac{U_d}{2}$ in presence of Zeeman field h obtained for $t_m = 0.25U_d$.

initial branches $\xi_d \pm U_d/2$ and for interconnecting two of them (internal ones).

3.3. Magnetization

Qualitative differences of the opposite spin spectra are indirectly manifested by the on-dot magnetization

$$m = \frac{1}{2}\left(\langle n_\downarrow\rangle - \langle n_\uparrow\rangle\right). \tag{42}$$

emerging outside the half-filling (see figure 7). To explain the sign change of QD magnetization, let us inspect equations (4)–(7), noting that Ψ_1 and Ψ_2 represent superpositions of the empty and singly occupied spin$-\downarrow$ configurations. Therefore, if for particular model parameters state Ψ_1 or Ψ_2 is the ground state, the dot magnetization would be oriented along the $\downarrow-$direction. In contrast, the states Ψ_3 and Ψ_4 are superpositions of the nonmagnetic $|\uparrow\downarrow\rangle$ state and the singly occupied spin$-\uparrow$ configuration. The ground state represented by Ψ_3 and Ψ_4 would then have magnetization along the $\uparrow-$direction. Figure 2 shows that for $\xi_d < 0$, the ground state of QD is represented by Ψ_3 or Ψ_4. This fact explains the sign change of the magnetization at half-filling, $\xi_d = 0$, in agreement with previous studies reported in [10, 11, 36].

As shown in the appendix (figure 13), the Zeeman field modifies the eigenenergies in such a way that, when aligned with the spin-down state, the crossing point between energies E_{12} and E_{34} shifts toward lower values of ξ_d (energies become equal at smaller ξ_d compared to the case without the field). This shift affects the polarization transition point of the magnetization. Specifically, for weak Zeeman fields (particularly when aligned with the spin-down orientation), the system favors spin-down polarization over a broader range of energies. Consequently, the magnetization turning point also occurs at lower energy levels ξ_d, as illustrated in figure 8. As the Zeeman field strength increases and surpasses a critical value (for $t_m = 0.25U_d$, this occurs at approximately $h > 0.25U_d$), the quantum dot's magnetization becomes polarized in a single direction over a wide range of energy levels ϵ_d. The results indicate that, in the presence of a strong Zeeman field, the only region where the quantum dot exhibits significant magnetization is when the magnetization is fully polarized in one direction. The transition point between opposite polarizations occurs at an energy where, beyond this point, the magnetization becomes very small. Therefore, in the region where the magnetization is substantial, it is aligned in a single direction. At this point, the system enters a regime where the external magnetic field dominates over the Majorana leakage influence, enforcing a rigid spin alignment.

3.4. Signatures of intersite pairing

The usual method for probing the QD quasiparticle spectrum relies on charge tunneling induced upon applying voltage between our setup and an external conducting tip. This sort of measurement has been reported by Deng *et al* [37], revealing enhancement of the zero-bias conductance.

Another method, proposed in [38], is based on equal spin Andreev scattering to detect efficiency of converting a given spin electron into a hole of the same polarization. The energy-dependent transmittance via such transport channel is given by $T_\sigma(\omega) = \Gamma_N^2\left(\left|\langle\langle \hat{d}_\sigma; \hat{f}\rangle\rangle_\omega\right|^2 + \left|\langle\langle \hat{f}; \hat{d}_\sigma\rangle\rangle_\omega\right|^2\right)$, where

Γ_N denotes the coupling of QD to the polarized conducting electrode. In the simplest approach, the influence of such an external reservoir would be responsible for a level-broadening. Under such conditions, we can express

$$\langle\langle \hat{d}_\downarrow;\hat{f}\rangle\rangle_\omega = \frac{1}{Z}\sum_{m,n,s,s'} \langle\Psi_n^s|\hat{d}_\downarrow|\Psi_m^{s'}\rangle\langle\Psi_m^{s'}|\hat{f}|\Psi_n^s\rangle \times \frac{e^{-\beta E_m^s}+e^{-\beta E_n^s}}{(\omega+i\Gamma_N)+E_n^s-E_m^s} \tag{43}$$

which accounts for the inter-site pairing of $\downarrow-$spin electrons. This Green's function (43) has the same poles as the single-particle propagator (25), but with different spectral weights. The matrix elements involving the states Ψ_1 and Ψ_2 that contribute to the zero-energy poles are given by

$$\langle\Psi_1^-|\hat{d}_\downarrow|\Psi_2^-\rangle\langle\Psi_2^-|\hat{f}|\Psi_1^-\rangle = u_p v_p^3 \tag{44}$$

$$\langle\Psi_1^+|\hat{d}_\downarrow|\Psi_2^+\rangle\langle\Psi_2^+|\hat{f}|\Psi_1^+\rangle = -u_p^3 v_p \tag{45}$$

$$\langle\Psi_2^-|\hat{d}_\downarrow|\Psi_1^-\rangle\langle\Psi_1^-|\hat{f}|\Psi_2^-\rangle = u_p^3 v_p \tag{46}$$

$$\langle\Psi_2^+|\hat{d}_\downarrow|\Psi_1^+\rangle\langle\Psi_1^+|\hat{f}|\Psi_2^+\rangle = -u_p v_p^3. \tag{47}$$

In a similar manner, the matrix elements involving Ψ_3 and Ψ_4 follow the same structure, with u_p and v_p replaced by u_q and v_q. Substituting the explicit form of $v_{p(q)}$ and $u_{p(q)}$, the sum of given matrix elements simplifies to $u_{p(q)}^3 v_{p(q)} + u_{p(q)} v_{p(q)}^3 = \frac{t_m}{E_{p(q)}}$. This leads to the following expression describing the amplitude of the zero-energy pole of the discussed Green's function

$$\frac{1}{Z}\left[\frac{2t_m}{E_p}\left(e^{-\beta E_1^-}-e^{-\beta E_1^+}\right)+\frac{2t_m}{E_q}\left(e^{-\beta E_3^-}-e^{-\beta E_3^+}\right)\right]. \tag{48}$$

The finite-energy poles of $\langle\langle \hat{d}_\sigma;\hat{f}\rangle\rangle_\omega$ are given by

$$\pm\frac{1}{Z}\frac{2t_m}{E_p}\left(e^{-\beta E_1^-}+e^{-\beta E_1^+}\right)\frac{1}{\omega+i\Gamma_N\pm E_p}, \tag{49}$$

$$\pm\frac{1}{Z}\frac{2t_m}{E_q}\left(e^{-\beta E_3^-}+e^{-\beta E_3^+}\right)\frac{1}{\omega+i\Gamma_N\pm E_q}. \tag{50}$$

A typical plot of the spin$-\downarrow$ selective Andreev transmittance is presented in figure 9 for several ratios t_m/U_d. These plots provide clear indication that zero-bias conductance of SESAR is able to probe the spectral weight of the Majorana mode as it varies against ξ_d. Again, we notice that the Coulomb repulsion shifts the optimal weight of such

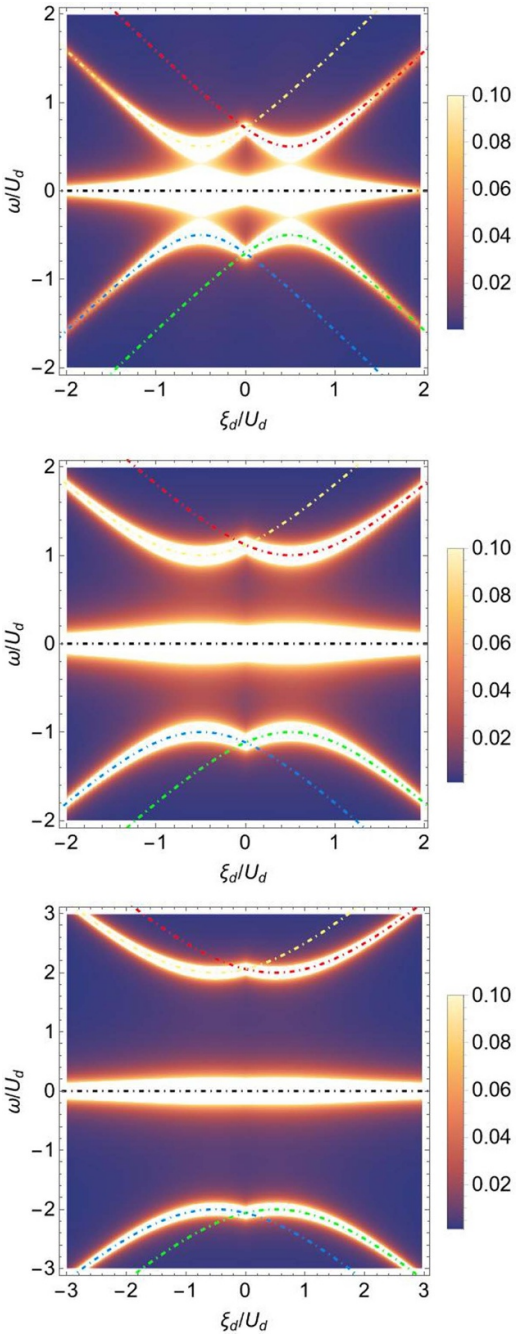

Figure 9. Transmittance of the selective equal spin Andreev reflection (SESAR) obtained for $t_m/U_d = 0.25$ (top panel), 0.5 (middle panel), and 1 (bottom panel), assuming temperature $k_bT = 0.01U_d$ and coupling $\Gamma_N = 0.01U_d$.

4. Results for $\epsilon_m \neq 0$

The local solution allows us to identify the origin of the quasiparticle spectrum of QD, assigning its specific features to the topological or trivial components. Such *identification* becomes a bit more complicated when $\epsilon_m \neq 0$. In such a situation, the eigenstates of our setup Ψ_i^s are nondegenerate, with the corresponding energies (8)–(11). In analogy to the quasiparticle energies (13) and (14), it is convenient to define

$$E_p^\pm = \sqrt{(\varepsilon_d \pm \epsilon_m)^2 + 4t_m^2} \tag{51}$$

$$E_q^\pm = \sqrt{(\varepsilon_d \pm \epsilon_m + U_d)^2 + 4t_m^2}. \tag{52}$$

which helps us to express the coefficients u_i^s appearing in the eigenstates $|\Psi_i^s\rangle$ by

$$\left(u_1^\pm\right)^2 = \frac{1}{2}\left(1 \pm \frac{\varepsilon_d+\epsilon_m}{E_p^+}\right), \tag{53}$$

$$\left(u_2^\pm\right)^2 = \frac{1}{2}\left(1 \pm \frac{\varepsilon_d-\epsilon_m}{E_p^-}\right), \tag{54}$$

$$\left(u_3^{\pm}\right)^2 = \frac{1}{2}\left(1 \pm \frac{\epsilon_m - \varepsilon_d + U_d}{E_q^-}\right), \tag{55}$$

$$\left(u_4^{\pm}\right)^2 = \frac{1}{2}\left(1 \pm \frac{\varepsilon_d + \epsilon_m + U_d}{E_q^+}\right), \tag{56}$$

and $(v_i^s)^2 = 1 - (u_i^s)^2$.

After algebraic calculations we obtain the following spectral function for arbitrary ϵ_m

$$\begin{aligned}
\rho_\downarrow(\omega) = {} & A_{12}^{-/-}\delta\left[\omega + \frac{1}{2}\left(E_p^- - E_p^+\right)\right] \\
& + A_{12}^{-/+}\delta\left[\omega - \frac{1}{2}\left(E_p^- + E_p^+\right)\right] \\
& + A_{12}^{+/-}\delta\left[\omega + \frac{1}{2}\left(E_p^- + E_p^+\right)\right] \\
& + A_{12}^{+/+}\delta\left[\omega - \frac{1}{2}\left(E_p^- - E_p^+\right)\right] \\
& + A_{34}^{-/-}\delta\left[\omega - \frac{1}{2}\left(E_q^- - E_q^+\right)\right] \\
& + A_{34}^{-/+}\delta\left[\omega - \frac{1}{2}\left(E_q^- + E_q^+\right)\right] \\
& + A_{34}^{+/-}\delta\left[\omega + \frac{1}{2}\left(E_q^- + E_q^+\right)\right] \\
& + A_{34}^{+/+}\delta\left[\omega + \frac{1}{2}\left(E_q^- - E_q^+\right)\right]
\end{aligned} \tag{57}$$

with the amplitudes $A_{12}^{s/s'}$ related to transitions $\Psi_1^s \leftrightarrow \Psi_2^{s'}$ given by

$$\begin{aligned}
A_{12}^{-/-} = {} & \frac{1}{Z}\left(u_1^- u_2^-\right)^2\left(e^{-\beta E_1^-} + e^{-\beta E_2^-}\right) \\
& + \frac{1}{Z}\left(v_1^+ v_2^+\right)^2\left(e^{-\beta E_1^+} + e^{-\beta E_2^+}\right), \\
A_{12}^{-/+} = {} & \frac{1}{Z}\left(u_1^- u_2^+\right)^2\left(e^{-\beta E_1^-} + e^{-\beta E_2^+}\right) \\
& + \frac{1}{Z}\left(v_1^- v_2^+\right)^2\left(e^{-\beta E_1^-} + e^{-\beta E_2^+}\right), \\
A_{12}^{+/-} = {} & \frac{1}{Z}\left(u_1^+ u_2^-\right)^2\left(e^{-\beta E_1^+} + e^{-\beta E_2^-}\right) \\
& + \frac{1}{Z}\left(v_1^+ v_2^-\right)^2\left(e^{-\beta E_1^+} + e^{-\beta E_2^-}\right), \\
A_{12}^{+/+} = {} & \frac{1}{Z}\left(u_1^+ u_2^+\right)^2\left(e^{-\beta E_1^+} + e^{-\beta E_2^+}\right) \\
& + \frac{1}{Z}\left(v_1^- v_2^-\right)^2\left(e^{-\beta E_1^-} + e^{-\beta E_2^-}\right)
\end{aligned} \tag{58}$$

and amplitudes $A_{34}^{s/s'}$ of transitions $\Psi_3^s \leftrightarrow \Psi_4^{s'}$ given by

$$\begin{aligned}
A_{34}^{-/-} = {} & \frac{1}{Z}\left(u_3^- u_4^-\right)^2\left(e^{-\beta E_3^-} + e^{-\beta E_4^-}\right) \\
& + \frac{1}{Z}\left(v_3^+ v_4^+\right)^2\left(e^{-\beta E_3^+} + e^{-\beta E_4^+}\right), \\
A_{34}^{-/+} = {} & \frac{1}{Z}\left(u_3^- u_4^+\right)^2\left(e^{-\beta E_3^-} + e^{-\beta E_4^+}\right) \\
& + \frac{1}{Z}\left(v_3^- v_4^+\right)^2\left(e^{-\beta E_3^-} + e^{-\beta E_4^+}\right), \\
A_{34}^{+/-} = {} & \frac{1}{Z}\left(u_3^+ u_4^-\right)^2\left(e^{-\beta E_3^+} + e^{-\beta E_4^-}\right) \\
& + \frac{1}{Z}\left(v_3^+ v_4^-\right)^2\left(e^{-\beta E_3^+} + e^{-\beta E_4^-}\right), \\
A_{34}^{+/+} = {} & \frac{1}{Z}\left(u_3^+ u_4^+\right)^2\left(e^{-\beta E_3^+} + e^{-\beta E_4^+}\right) \\
& + \frac{1}{Z}\left(v_3^- v_4^-\right)^2\left(e^{-\beta E_3^-} + e^{-\beta E_4^-}\right).
\end{aligned} \tag{59}$$

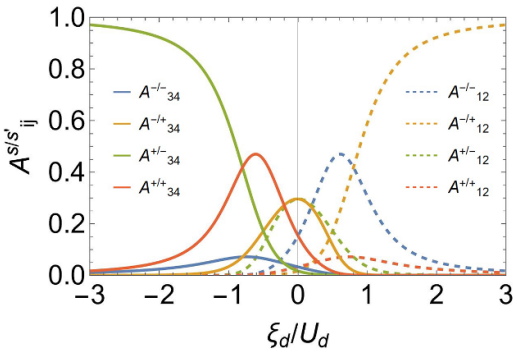

Figure 10. Variation of the transition probabilities $A_{ij}^{s/s'}$ between Ψ_i^s and $\Psi_j^{s'}$ states plotted against $\xi_d = \varepsilon_d + U_d/2$. Results are obtained for $t_m/U_d = 0.3$, assuming a finite overlap between the edge states $\epsilon_m = 0.3U_d$.

For $\epsilon_m \neq 0$ we obtain nondegenerate eigenfunctions, characterized by 8 quasiparticle excitation energies. The transitions from each $|\Psi_i\rangle$ to $|\Psi_j\rangle$ are always accompanied by the corresponding transitions from $|\Psi_j\rangle$ to $|\Psi_i\rangle$ (with interchanged upper indexes), contributing to the quasiparticle energy. For instance, the transition $|\Psi_1^-\rangle \to |\Psi_2^-\rangle$ contributes to the same pole as $|\Psi_2^+\rangle \to |\Psi_1^+\rangle$. Although in general $\rho_\downarrow(\omega)$ is characterized by 8 quasiparticle energies, in practice all of them are visible only in close vicinity of the half-filling, $\xi_d \simeq 0$. Outside of this region, some amplitudes become negligible and the spectrum of $\downarrow$-spin electrons is represented by four quasiparticles (figures 10 and 11). Far away from the half-filling, $|\xi_d| \gg U_d$, one pair disappears as well, and the spectrum simplifies to the standard single quasiparticle.

In figure 11 we plot the density of states $\rho_\downarrow(\omega)$ for nonvanishing ϵ_m, which resembles the bowtie shapes obtained earlier [8] from the mean-field approximation. Under specific conditions, $\xi_d = \pm\frac{U_d}{2}$, we observe a crossing of the Majorana features, which otherwise are split into bonding/antibonding energies. At half-filling, the quasiparticle energies related to transitions $|\Psi_1^s\rangle \leftrightarrow |\Psi_2^{s'}\rangle$ are identical to the quasiparticle energies for transitions $|\Psi_3^s\rangle \leftrightarrow |\Psi_4^{s'}\rangle$, i.e. $E_p^s = E_q^s$. Consequently, the trivial and topological features are represented by four peaks at $\frac{1}{2}(\pm E_p^- \pm E_p^+)$ and $\frac{1}{2}(\pm E_q^- \pm E_q^+)$.

Nonvanishing ϵ_m also modifies the spectrum of electrons that are not directly coupled to MZM. Figure 12 shows that when a nonzero ϵ_m is introduced, the spectrum of $\uparrow$ electrons generally exhibits an 8-peak structure (marked by different

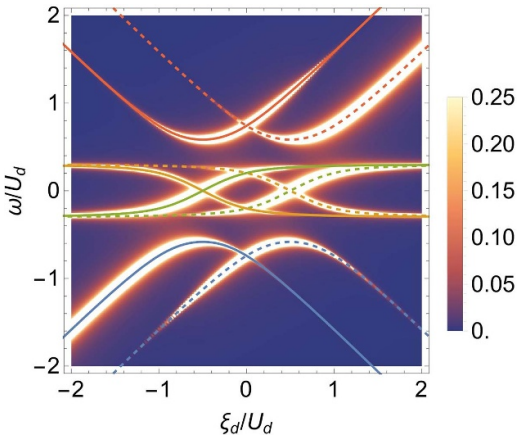

Figure 11. Variation of the quasiparticle spectrum $\rho_{d\downarrow}(\omega)$ with respect to $\xi_d = \varepsilon_d + U_d/2$ obtained for $t_m = 0.25U_d$ and $\epsilon_m = 0.3U_d$. The position of poles related to transitions between Ψ_1 and Ψ_2 states is marked with dashed lines, whereas transitions between Ψ_3 and Ψ_4 are marked with solid ones.

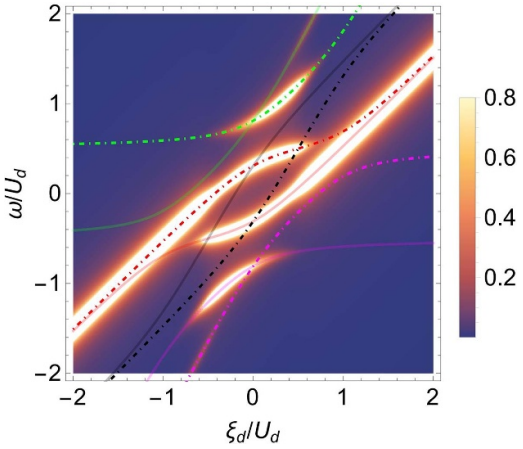

Figure 12. Variation of the quasiparticle spectrum $\rho_{d\uparrow}(\omega)$ with respect to $\xi_d = \varepsilon_d + U_d/2$ obtained for $t_m = 0.25U_d$ and $\epsilon_m = 0.3U_g$. Position of poles related to transitions between Ψ_2 and Ψ_3 states are marked with dashed lines whereas transitions between Ψ_1 and Ψ_4 are marked with solid faded ones.

color lines). However, four of these peaks have small amplitude across the entire energy range, while 2 additional peaks display significant amplitude only near half-filling. As a result, close to half-filling, we observe 4 well-pronounced peaks, whereas far from half-filling, only 2 peaks remain.

5. Summary and outlook

We have studied the spectrum of the single quantum dot coupled to the boundary modes of the topological superconductor. From the exact solution of this setup, we inferred the energies and spectral weights of the leaking Majorana mode(s) coexisting with the conventional (nontopological) quasiparticles.

For the non-correlated case, the trivial quasiparticles exist at energies $\pm\sqrt{\varepsilon_d^2 + 4t_m^2}$. In this scenario, the optimal amplitude of the zero-energy mode occurs for $\varepsilon_d = 0$. Under such circumstances, the Majorana mode acquires half of the total spectral weight, and the trivial quasiparticles equally share the remaining amount. The spectral function of QD in this case is represented by a three-peak structure $\rho_\downarrow(\omega) = 0.5\delta(\omega) + 0.25\delta(\omega - 2t_m) + 0.25\delta(\omega + 2t_m)$. Away from half-filling, one of the trivial quasiparticles gradually absorbs more and more spectral weight, at the expense of both the other conventional quasiparticle and the zero-energy mode.

In the presence of the Coulomb repulsion, a leakage of the zero-energy mode is most efficient when the zero mode coincides either with the energy level $\varepsilon_d = 0$ or with the Coulomb satellite $\varepsilon_d + U_d = 0$ (i.e. $\xi_d = \pm\frac{U_d}{2}$). One should note that, at such points, the trivial quasiparticles are formed at $\pm 2t_m$, provided that the Majorana modes do not overlap with one another. Away from these points, the spectrum of $\downarrow$-spin electrons consists of four trivial quasiparticles coexisting with the zero-energy mode (figure 3). We have demonstrated that they could be experimentally detected by spin-polarized Andreev spectroscopy, figure 9. The spin-$\uparrow$ sector also consists of four quasiparticle branches, but all of them refer to the nontopological states.

We also investigated the quantum dot spectrum for the case of a short topological superconductor, where the Majorana modes overlap with one another. In such a situation, the boundary modes transmitted onto the correlated quantum dot form two sets of bonding/antibonding states separated from the remaining four trivial quasiparticle branches, figure 11. Again, the optimal spectral weight of the topological quasiparticles coincides with $\xi_d = \pm\frac{U_d}{2}$. Near these special points, the Majorana modes cross each other, forming a bowtie shape.

Our analytical study extends the previous results [7] obtained within the Hubbard-I approximation. The expressions obtained here could be a useful starting point for further considerations of the many-body effects arising from the coupling of QD-MBS to mobile electrons of the external lead(s). They would also be helpful for investigating far-from-equilibrium effects, which can be induced by imposing quantum quench and/or periodic driving.

Data availability statement

The data that support the findings of this study are openly available at the following URL/DOI: https://zenodo.org/records/13936579 [39].

Acknowledgments

This research project has been supported by National Science Centre (Poland) through the Grant No. 2022/04/Y/ST3/00061.

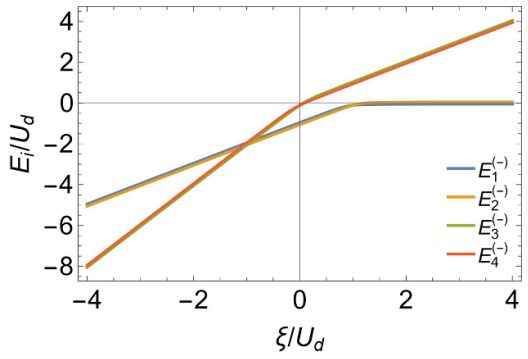

Figure 13. Dependence of the eigenenergies E_i^- on the energy level ε_d of QD in Zeeman field $h = 0.5U_d$ obtained for weak overlap $\epsilon_m = 0.1U_d$.

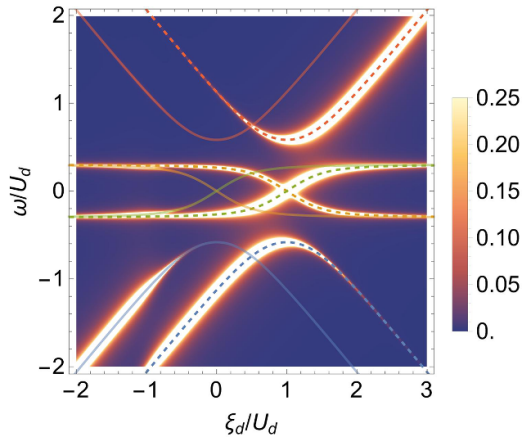

Figure 14. Variation of the quasiparticle spectrum $\rho_{d\downarrow}(\omega)$ with respect to $\xi_d = \varepsilon_d + U_d/2$ obtained for the same set of parameters as in figure 11 and Zeeman field $h = 0.5U_d$. The position of poles related to transitions between Ψ_1 and Ψ_2 states is marked with dashed lines, whereas transitions between Ψ_3 and Ψ_4 are marked with faded solid ones.

Appendix: Influence of Zeeman field

In the presence of the external magnetic field, h, the Hamiltonian of QD takes the form

$$\hat{H}_{\mathrm{QD}} = (\varepsilon_d + h)\hat{d}_\uparrow^\dagger \hat{d}_\uparrow + (\varepsilon_d - h)\hat{d}_\downarrow^\dagger \hat{d}_\downarrow + U_d \hat{n}_\uparrow \hat{n}_\downarrow, \qquad \text{(A.1)}$$

where $\epsilon_\downarrow = \epsilon_d - h$, $\epsilon_\uparrow = \epsilon_d + h$ yield the eigenvalues (11)

$$E_1^\pm = \frac{1}{2}\left[\epsilon_\downarrow \pm \sqrt{(\epsilon_\downarrow + \epsilon_m)^2 + 4t_m^2}\right] \qquad \text{(A.2)}$$

$$E_2^\pm = \frac{1}{2}\left[\epsilon_\downarrow \pm \sqrt{(\epsilon_\downarrow - \epsilon_m)^2 + 4t_m^2}\right] \qquad \text{(A.3)}$$

$$E_3^\pm = \frac{1}{2}\left[\epsilon_\downarrow + 2\epsilon_\uparrow + U_d \pm \sqrt{(\epsilon_\downarrow - \epsilon_m + U_d)^2 + 4t_m^2}\right] \qquad \text{(A.4)}$$

$$E_4^\pm = \frac{1}{2}\left[\epsilon_\downarrow + 2\epsilon_\uparrow + U_d \pm \sqrt{(\epsilon_\downarrow + \epsilon_m + U_d)^2 + 4t_m^2}\right]. \qquad \text{(A.5)}$$

Coefficients u_i^s and v_i^s remain the same upon substituting ϵ_d by $\epsilon_\downarrow$.

A magnetic field parallel to $\downarrow$ spin causes lowering of energies E_1 and E_2. Conversely, $E_{3,4}$ have higher energies. This shifts the transition point from the half-filling condition. The Zeeman field shifts all quasiparticle peaks in both spin sectors, which can be seen in figure 14. Additionally, we notice that the magnetic field reduces the amplitudes of transitions between $\Psi_{3,4}$.

ORCID iDs

Jan Barański https://orcid.org/0000-0002-0963-497X
Magdalena Barańska https://orcid.org/0000-0003-1964-6373
Tadeusz Domański https://orcid.org/0000-0003-1977-3989

References

[1] Liu D E and Baranger H U 2011 Detecting a Majorana-fermion zero mode using a quantum dot *Phys. Rev.* B **84** 201308
[2] Deng M T, Vaitiekėnas S, Hansen E B, Danon J, Leijnse M, Flensberg K, Nygård J, Krogstrup P and Marcus C M 2016 Majorana bound state in a coupled quantum-dot hybrid-nanowire system *Science* **354** 1557–62
[3] Li Z-Z, Lam C-H and You J Q 2015 Probing Majorana bound states via counting statistics of a single electron transistor *Sci. Rep.* **5** 11416
[4] Liu D E, Cheng M and Lutchyn R M 2015 Probing Majorana physics in quantum-dot shot-noise experiments *Phys. Rev.* B **91** 081405
[5] Gong W-J, Zhang S-F, Li Z-C, Yi G and Zheng Y-S 2014 Detection of a Majorana fermion zero mode by a t-shaped quantum-dot structure *Phys. Rev.* B **89** 245413
[6] Leijnse M 2014 Thermoelectric signatures of a majorana bound state coupled to a quantum dot *New J. Phys.* **16** 015029
[7] Ricco L S, de Souza M, Figueira M S, Shelykh I A and Seridonio A C 2019 Spin-dependent zero-bias peak in a hybrid nanowire-quantum dot system: distinguishing isolated Majorana fermions from Andreev bound states *Phys. Rev.* B **99** 155159
[8] Prada E, Aguado R and San-Jose P 2017 Measuring Majorana nonlocality and spin structure with a quantum dot *Phys. Rev.* B **96** 085418
[9] Vernek E, Penteado P H, Seridonio A C and Egues J C 2014 Subtle leakage of a Majorana mode into a quantum dot *Phys. Rev.* B **89** 165314
[10] Lee M, Lim J S and López R 2013 Kondo effect in a quantum dot side-coupled to a topological superconductor *Phys. Rev.* B **87** 241402
[11] Cheng M, Becker M, Bauer B and Lutchyn R M 2014 Interplay between Kondo and Majorana interactions in quantum dots *Phys. Rev.* X **4** 031051
[12] Chirla R, Dinu I V, Moldoveanu V and Moca C P 2014 Transport in a hybrid normal metal/topological superconductor Kondo model *Phys. Rev.* B **90** 195108
[13] Shankar G and Maciejko J 2019 Exactly solvable Majorana-Anderson impurity models *Phys. Rev.* B **100** 241105
[14] Silva J F, da Silva L G G V D and Vernek E 2020 Robustness of the Kondo effect in a quantum dot coupled to Majorana zero modes *Phys. Rev.* B **101** 075428
[15] Ramos-Andrade J P, Orellana P A and Vernek E 2020 Majorana bound state in the continuum: Coupling between

a Majorana bound state and a quantum dot mediated by a continuum energy spectrum *Phys. Rev.* B **101** 115403
[16] Medina-Cuy F, Martínez D, Domínguez-Adame F and Orellana P A 2023 Majorana bound states in a driven quantum dot *Eur. Phys. J. Plus* **138** 701
[17] Zienkiewicz T, Barański J, Górski G and Domański T 2020 Leakage of Majorana mode into correlated quantum dot nearby its singlet-doublet crossover *J. Phys.: Condens. Matter* **32** 025302
[18] Valentini M, Borovkov M, Prada E, Martí-Sánchez S, Botifoll M, Hofmann A, Arbiol J, Aguado R, San-Jose P and Katsaros G 2022 Majorana-like coulomb spectroscopy in the absence of zero-bias peaks *Nature* **612** 442–7
[19] Chen J, Woods B, Yu P, Hocevar M, Car D, Plissard S, Bakkers E, Stanescu T and Frolov S 2019 Ubiquitous non-majorana zero-bias conductance peaks in nanowire devices *Phys. Rev. Lett.* **123** 107703
[20] Hess R, Legg H F, Loss D and Klinovaja J 2021 Local and nonlocal quantum transport due to andreev bound states in finite rashba nanowires with superconducting and normal sections *Phys. Rev.* B **104** 075405
[21] Liu C-X, Sau J D, Stanescu T D and Sarma S D 2017 Andreev bound states versus Majorana bound states in quantum dot-nanowire-superconductor hybrid structures: trivial versus topological zero-bias conductance peaks *Phys. Rev.* B **96** 075161
[22] Golub A, Kuzmenko I and Avishai Y 2011 Kondo correlations and majorana bound states in a metal to quantum-dot to topological-superconductor junction *Phys. Rev. Lett.* **107** 176802
[23] Weymann I and Wójcik K P 2017 Transport properties of a hybrid Majorana wire-quantum dot system with ferromagnetic contacts *Phys. Rev.* B **95** 155427
[24] Majek P and Weymann I 2024 Spin-selective transport in a correlated double quantum dot-majorana wire system *Sci. Rep.* **14** 17762
[25] He J J, Ng T, Lee P A and Law K 2014 Selective equal-spin andreev reflections induced by Majorana fermions *Phys. Rev. Lett.* **112** 037001
[26] Sun H-H *et al* 2016 Majorana zero mode detected with spin selective andreev reflection in the vortex of a topological superconductor *Phys. Rev. Lett.* **116** 257003
[27] Zhang K, Zeng J, Dong X and Cheng Q 2018 Spin dependence of crossed andreev reflection and electron tunneling induced by Majorana fermions *J. Phys.: Condens. Matter* **30** 505302
[28] Głodzik S, Sedlmayr N and Domański T 2020 How to measure the Majorana polarization of a topological planar josephson junction *Phys. Rev.* B **102** 085411
[29] Dvir T *et al* 2023 Realization of a minimal kitaev chain in coupled quantum dots *Nature* **614** 445–50
[30] Souto R S, Tsintzis A, Leijnse M and Danon J 2023 Probing Majorana localization in minimal kitaev chains through a quantum dot *Phys. Rev. Res.* **5** 043182
[31] Wang G *et al* 2022 Singlet and triplet cooper pair splitting in hybrid superconducting nanowires *Nature* **612** 448–53
[32] Zeng J, He J J, Ning Z, Xu D-H and Wang R 2024 Spin signature of Majorana fermions in topological nodal-point superconductors (arXiv:2403.02036v2)
[33] Leijnse M and Flensberg K 2011 Scheme to measure Majorana fermion lifetimes using a quantum dot *Phys. Rev.* B **84** 140501
[34] Bauer J, Oguri A and Hewson A C 2007 Spectral properties of locally correlated electrons in a Bardeen–Cooper–Schrieffer superconductor *J. Phys.: Condens. Matter* **19** 486211
[35] Barański J and Domański T 2013 In-gap states of a quantum dot coupled between a normal and a superconducting lead *J. Phys.: Condens. Matter* **25** 435305
[36] Huguet A, Wrześniewski K and Weymann I 2023 Spin effects on transport and zero-bias anomaly in a hybrid Majorana wire-quantum dot system *Sci. Rep.* **13** 17279
[37] Deng M-T, Vaitiekėnas S, Prada E, San-Jose P, Nygård J, Krogstrup P, Aguado R and Marcus C M 2018 Nonlocality of Majorana modes in hybrid nanowires *Phys. Rev.* B **98** 085125
[38] He J J, Ng T K, Lee P A and Law K T 2014 Selective equal-spin Andreev reflections induced by Majorana fermions *Phys. Rev. Lett.* **112** 037001
[39] Barański J Barańska M Zienkiewicz T and Domanski T 2024 Interplay of correlations and Majorana mode from local solution perspective *Zenodo* https://doi.org/10.5281/zenodo.13936579